Continuum Λ spectra for a $^{6}_{\Lambda}$Li hypernucleus in the ^{6}Li(K^-, π^-) reaction

Toru Harada [1,2,*] and Yoshiharu Hirabayashi [3]

[1] *Center for Physics and Mathematics, Osaka Electro-Communication University, Neyagawa, Osaka 572-8530, Japan*
[2] *J-PARC Branch, KEK Theory Center, Institute of Particle and Nuclear Studies, High Energy Accelerator Research Organization (KEK), 203-1, Shirakata, Tokai, Ibaraki 319-1106, Japan*
[3] *Information Initiative Center, Hokkaido University, Sapporo 060-0811, Japan*

(Received 14 March 2025; revised 7 May 2025; accepted 20 May 2025; published 17 June 2025)

We theoretically investigate Λ production via a (K^-, π^-) reaction on a ^{6}Li target, using the distorted-wave impulse approximation with a Fermi-averaged $K^-n \to \pi^-\Lambda$ amplitude. We calculate Λ production spectra using the Green's function method for a ^{5}Li nuclear core + Λ system, employing a Λ folding-model potential based on the ^{5}Li nuclear density, which is constructed from α-p and ^{3}He-d cluster wave functions. The results show that the calculated spectrum, which includes Λ bound, resonance, and continuum states, agrees well with the experimental data from the (K^-, π^-) reaction at $p_{K^-} = 790$ MeV/c (0°), where substitutional $(0p,\ 0p^{-1})_{\Lambda n}$ and $(0s,\ 0s^{-1})_{\Lambda n}$ configurations dominate in the near-recoilless reactions. A narrow peak corresponds to a high-lying excited state with spin-parity $J^P = 1^+$ at $E_\Lambda = 13.8$ MeV near the ^{3}He + d + Λ threshold, arising from interference effects between ^{5}Li$(3/2^+) \otimes (0s_{1/2})_\Lambda$ and ^{5}Li$(1/2^+) \otimes (0s_{1/2})_\Lambda$ components. This study offers a valuable framework for extracting essential information on the structure and production mechanisms of hypernuclear states from experimental data.

DOI: 10.1103/9c6g-dsq2

I. INTRODUCTION

Recently, the J-PARC E10 Collaboration [1] demonstrated the absence of a bound state for the neutron-rich $^{6}_{\Lambda}$H hypernucleus in a (π^-, K^+) reaction on a ^{6}Li target [2]. Additionally, the analysis of the continuum spectrum data [3] indicated that the Σ^--^{5}He potential is repulsive, with a strength of $U_\Sigma = +30$ MeV. The J-PARC E75 Collaboration [4] has conducted a search for the Ξ hypernucleus $^{7}_{\Xi}$H via a (K^-, K^+) reaction on a ^{7}Li target to investigate the properties of the yet unsettled Ξ nuclear potential. A search for $^{6}_{\Xi}$H using the (K^-, K^+) reaction on a ^{6}Li target has also been proposed at J-PARC.

One of the primary objectives of this study is to elucidate the structure and production mechanisms of hypernuclei by theoretically analyzing experimental spectra from (K^-, π^-), (π^+, K^+), and (K^-, K^+) reactions. As an initial step toward achieving this goal, we aim to establish an effective method for analyzing Λ production spectra, including both bound and continuum states, for Λ hypernuclei whose overall characteristics are already well understood.

The (K^-, π^-) reaction has played a crucial role in elucidating the structure of Λ hypernuclear excited states by inducing a small momentum transfer of $q \simeq 60$–80 MeV/c to a Λ hyperon [5–7]. This reaction has allowed the observation of prominent peaks corresponding to "substitutional states" in Λ hypernuclei in experimental data on light nuclear targets [7–11]. The Heidelberg-Saclay-Strasbourg Collaboration [10,11] has reported that the ^{6}Li(K^-, π^-) reaction at $p_{K^-} =$ 790 MeV/c and $\theta_{\rm lab} = 0°$ reveals two prominent peaks at $E_\Lambda = 3.8$ and 13.8 MeV, measured relative to the ^{5}Li(g.s.) + Λ threshold, as shown in Fig. 1. These peaks are identified as states with spin-parity $J^P = 1^+$ in a $^{6}_{\Lambda}$Li hypernucleus, corresponding to substitutional $(0p,\ 0p^{-1})_{\Lambda n}$ and $(0s,\ 0s^{-1})_{\Lambda n}$ configurations [11]. This is attributed to the dominance of an angular-momentum transfer of $\Delta L = 0$ in the near-recoilless (K^-, π^-) reactions on a ^{6}Li(1^+; g.s.) target. In Fig. 1, we also include data from the proton-coincidence nonmesonic weak decay of $^{5}_{\Lambda}$He, obtained from the π^- spectrum in a $^{5}_{\Lambda}$He lifetime measurement using the ^{6}Li(K^-, π^-) reaction at $p_{K^-} =$ 800 MeV/c [12]. Notably, the small yield from $^{6}_{\Lambda}$Li(1^+) at 13.8 MeV is comparable to that from $^{6}_{\Lambda}$Li(g.s.) at -4.5 MeV. These data suggest a minimal (∼4%) admixture of (α-p)-Λ to (^{3}He -d)-Λ in $^{6}_{\Lambda}$Li, whose wave functions exhibit the spatial symmetries of $[f] = [411]$ and [321] in the Young's scheme [13], respectively, as discussed by Majling *et al.* [14].

Many authors [15–17] have theoretically studied spectroscopy of p-shell Λ hypernuclei in (K^-, π^-), (π^+, K^+), and (e, $e'K^+$) reactions, using a distorted-wave impulse approximation. Shell-model [14,18] and cluster-model [19–21] descriptions discussed the structure and production of $^{6}_{\Lambda}$Li via the ^{6}Li(K^-, π^-) reaction within a bound-state approximation. Auerbach and Van Giai [22] studied basic gross features of continuum effects considering ΛN^{-1} configurations in the (K^-, π^-) reaction on ^{6}Li, together with ^{7}Li and ^{9}Be.

In this paper, we theoretically investigate Λ production via the (K^-, π^-) reaction on a ^{6}Li target, using the distorted-wave impulse approximation with the Fermi-averaged $K^-n \to \pi^-\Lambda$ amplitudes incorporating nuclear medium effects. To describe Λ bound, resonance, and continuum states for

*Contact author: harada@osakac.ac.jp

 ©2025 American Physical Society

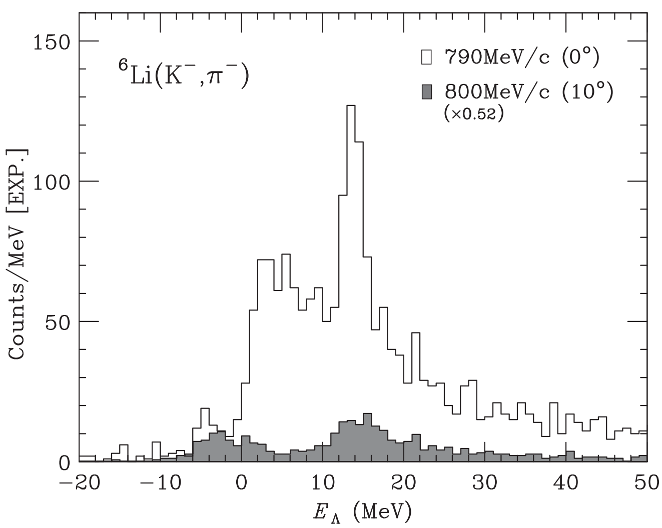

FIG. 1. Experimental data from the ^{6}Li(K^-, π^-) reaction at $p_{K^-} = 790$ MeV/c and $\theta_{\rm lab} = 0°$ [10], as a function of E_Λ measured relative to the ^{5}Li(g.s.) + Λ threshold, together with the data from the proton-coincidence nonmesonic weak decay of $^5_\Lambda$He, obtained from the π^- spectrum in a $^5_\Lambda$He lifetime measurement using the ^{6}Li(K^-, π^-) reaction at $p_{K^-} = 800$ MeV/c [12]. The latter dataset is normalized by multiplying a factor of 0.52 at the −2.5 MeV data point for comparison.

$^6_\Lambda$Li, we calculate a Λ production spectrum by employing the Green's function method [23], which provides a comprehensive description of Λ-nucleus dynamics to potential interactions. We obtain the Λ folding-model potentials with the ^{5}Li nuclear densities based on α-p and ^{3}He-d cluster wave functions. We examine the shape and magnitude of the Λ production spectra, comparing them with the experimental data [10]. This study aims to extract essential information on the structure and production mechanisms of $^6_\Lambda$Li from the data of the ^{6}Li(K^-, π^-) reaction.

II. METHOD

A. Distorted-wave impulse approximation

The double-differential cross section for Λ production on a nuclear target in the (K^-, π^-) reaction is often calculated using the distorted-wave impulse approximation (DWIA) [15,24]. According to the Green's function method [23], the double-differential laboratory cross section on a nuclear target with spin J_A and its z component M_A [24] can be expressed as follows (in natural units, $\hbar = c = 1$):

$$\frac{d^2\sigma}{d\Omega dE} = \frac{1}{[J_A]} \sum_{M_A} S(E_B), \tag{1}$$

where $[J_A] = 2J_A + 1$ and $S(E_B)$ is the strength function, which is given by

$$S(E_B) = -\frac{1}{\pi} {\rm Im} \sum_{cc'} \int d\boldsymbol{r} d\boldsymbol{r}' F_c^{\Lambda\dagger}(\boldsymbol{r}) G_{cc'}(E_B; \boldsymbol{r}, \boldsymbol{r}') F_{c'}^{\Lambda}(\boldsymbol{r}'), \tag{2}$$

as a function of the energy E_B for hypernuclear final states. Here $G_{cc'}$ is a coupled-channels (CC) Green's function [25] that accounts for spin couplings between hypernuclear states, where c (c') denotes a complete set of eigenstates of the system. The Λ production amplitude F_c^Λ is defined as

$$F_c^\Lambda = \beta^{\frac{1}{2}} \overline{f}_{K^-n\to\pi^-\Lambda} \chi_{\boldsymbol{p}\pi}^{(-)*} \chi_{\boldsymbol{p}K}^{(+)} \langle c \,|\hat{\psi}_n|\, \Psi_A \rangle, \tag{3}$$

where $\chi_{\boldsymbol{p}\pi}^{(-)}$ and $\chi_{\boldsymbol{p}K}^{(+)}$ are the distorted waves for the outgoing π^- and incoming K^- mesons, respectively. The function $\langle c \,|\hat{\psi}_n|\, \Psi_A \rangle$ represents the hole-state wave function for a struck neutron in the target. The quantity $\overline{f}_{K^-n\to\pi^-\Lambda}$ is the Fermi-averaged amplitude for the $K^-n \to \pi^-\Lambda$ reaction in the nuclear medium [26,27], and β is a kinematical factor converting from the two-body K^--nucleon (N) laboratory system to the K^--nucleus laboratory system [28,29]. The energy and momentum transfer are given by

$$\omega = E_K - E_\pi, \quad \boldsymbol{q} = \boldsymbol{p}_K - \boldsymbol{p}_\pi, \tag{4}$$

where $E_K = (\boldsymbol{p}_K^2 + m_K^2)^{1/2}$ and $E_\pi = (\boldsymbol{p}_\pi^2 + m_\pi^2)^{1/2}$. Here $\boldsymbol{p}_K$ and m_K ($\boldsymbol{p}_\pi$ and m_π) denote the laboratory momenta and rest masses of K^- and π^-, respectively.

The distorted waves, $\chi_{\boldsymbol{p}\pi}^{(-)}$ and $\chi_{\boldsymbol{p}K}^{(+)}$, in Eq. (3) are estimated using the eikonal approximation, with total cross sections of $\sigma_K = 30$ mb for K^-N and $\sigma_\pi = 32$ mb for π^-N, and distortion parameters $\alpha_K = \alpha_\pi = 0$ [26]. Recoil effects are also incorporated, leading to an effective momentum transfer $q_{\rm eff} \simeq (1 - 1/A)q \simeq 0.83q$ for a light nuclear system with $A = 6$.

B. Model wave functions

For a ^{6}Li(1^+; g.s.) target, the wave function is expressed in the $\alpha + d$ cluster model [30],

$$\Psi_A^{(^6{\rm Li})} = \mathcal{A}\big[[\phi_\alpha \phi_d]_{1^+} \otimes \chi_{L_A}^{(\alpha\text{-}d)}\big]_{J_A}, \tag{5}$$

where $\mathcal{A}$ is an antisymmetrization operator; ϕ_α and ϕ_d are the internal wave functions of α and d, respectively; and $\chi_{L_A}^{(\alpha\text{-}d)}$ is the relative wave function between α and d. Here we use a $(0s)^4$ harmonic oscillator wave function for ϕ_α with a size parameter $b_\alpha = 1.39$ fm and a $(0s)^2$ wave function for $\phi_d = c_1\phi_1 + c_2\phi_2$, where $\phi_i = \exp\{-(r/2b_i)^2\}$ with $c_1 = 0.07197$, $c_2 = 0.05090$, $b_1 = 1.105$ fm, and $b_2 = 2.395$ fm, incorporating the distortion effect in d [31]. According to the orthogonality condition model [30] with an appropriate α-d potential [32], we obtain the relative wave function $\chi_{L_A}^{(\alpha\text{-}d)}$ with an orbital angular momentum of $L_A = 0$ and a binding energy of 1.47 MeV relative to the $\alpha + d$ threshold. The charge root-mean-square (rms) radius of ^{6}Li(1^+; g.s.) is obtained as 2.53 fm, which is in good agreement with the experimental value of 2.56 ± 0.05 fm from electron elastic scatterings [33].

The wave function $\langle c \,|\hat{\psi}_n|\, \Psi_A \rangle$ for a neutron p-hole or s-hole state in Eq. (3) can be determined as a spectroscopic amplitude describing the ℓ_N-neutron pickup from ^{6}Li(1^+; g.s.) in the $\alpha + d$ cluster model. Table I lists the values of the input energies ϵ_N and widths Γ, as well as the spectroscopic factors S_{ℓ_N} for the neutron $0p^{-1}$ and $0s^{-1}$ orbits, based on the experimental data from the ^{6}Li(p, $2p$) reaction [34,35].

TABLE I. Calculated and input values of neutron $0p^{-1}$ and $0s^{-1}$ states for ^{6}Li(1^+; g.s.). ϵ_N and $\langle r^2\rangle^{1/2}$ denote energies and rms radii for the neutron-hole states, respectively, which are given by spectroscopic amplitudes in a $\alpha + d$ cluster model. The width Γ and spectroscopic factor S_{ℓ_N} for these states are taken from the experimental data [34,35].

State	ϵ_N (MeV)	$\langle r^2\rangle^{1/2}$ (fm)	Γ (MeV)	S_{ℓ_N}
$0p^{-1}$	−4.5	3.58	1.2[a]	0.8[b]
$0s^{-1}$	−21.3	2.34	0.2[a]	1.6[b]

[a]Reference [34].
[b]Reference [35].

For $^6_\Lambda$Li hypernuclear final states, we employ multiconfigurational wave functions in a ^{5}Li nuclear core + Λ model, which are expressed as

$$\Psi_{J_B}^{(^6_\Lambda\mathrm{Li})} = \sum_c \left[\Phi_{J_C}^{(^5\mathrm{Li})} \otimes \varphi_{j\ell s}^{(\Lambda)}(\boldsymbol{r})\right]_{J_B}, \tag{6}$$

where the abbreviation $c = \{J_C j\ell s\}$, $\Phi_{J_C}^{(^5\mathrm{Li})}$ denotes the wave function for ^{5}Li with spin J_C, $\varphi_{j\ell s}^{(\Lambda)}$ represents the relative wave function with the $(j\ell s)$ state, and $\boldsymbol{r}$ is the relative coordinate between ^{5}Li(J_C) and Λ. Since non-spin-flip processes predominantly occur in $K^- n \to \pi^- \Lambda$ reactions at $p_{K^-} =$ 700–800 MeV/c, we consider hypernuclear final states of $^6_\Lambda$Li with $J^P = (1^+ \otimes \Delta L) = 1^+, 0^-, 1^-, 2^-, 1^+, 2^+, 3^+, \cdots$, which correspond to configurations of $^5\mathrm{Li}(J_C) \otimes \Lambda$, where $\Delta L = 0, 1, 2, \cdots$, as the angular momentum transfer to the ^{6}Li(1^+; g.s.) target in the (K^-, π^-) reaction.

Figure 2 presents the experimental energy levels and associated decay thresholds of $^6_\Lambda$Li [10], together with those of

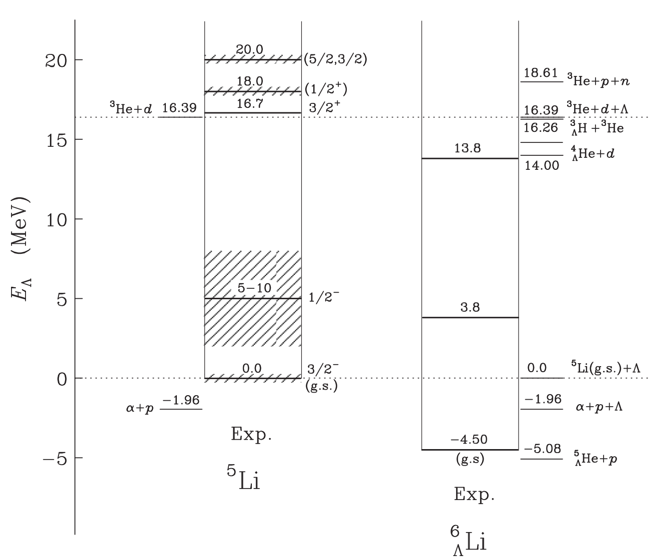

FIG. 2. Experimental energy levels of $^6_\Lambda$Li and the related decay thresholds, as a function of E_Λ measured from the ^{5}Li(g.s.) + Λ threshold, together with those of ^{5}Li as a core nucleus [36]. The data are taken from Ref. [10].

^{5}Li [36]. In this study, we measure the Λ energy E_Λ measured relative to the ^{5}Li(g.s.) + Λ threshold, which is defined as

$$E_\Lambda = E_B - M(^5\mathrm{Li(g.s.)}) - m_\Lambda = -B_\Lambda, \tag{7}$$

where $M(^5\mathrm{Li(g.s.)})$ and m_Λ are the masses of ^{5}Li(g.s.) and Λ, respectively. We note that a low-lying narrow $3/2^-$ resonance state of ^{5}Li(g.s.) exists at $(E_r, \Gamma) =$ (1.96 MeV, 0.65 MeV) above the $\alpha + p$ threshold, while a broad state of ^{5}Li($1/2^-$) is located at 5–10 MeV [34], corresponding to the valence $0p_{3/2}$ and $0p_{1/2}$ proton orbits in the α-p configurations, respectively. On the other hand, high-lying resonance states, ^{5}Li($3/2^+$) at 16.7 MeV and ^{5}Li($1/2^+$) at 18.0 MeV, near the ^{3}He $+d$ threshold, are expected to be described by the ^{3}He -d configurations.

C. Coupled-channels calculations

To investigate Λ-nucleus dynamics within this model space, we obtain the wave functions $\varphi_{j\ell s}^{(\Lambda)}$ in Eq. (6) by solving the following CC equation with a Λ-nucleus optical potential $\hat{U}_\Lambda$:

$$\left[-\frac{1}{2\mu_c}\nabla^2 + U_{cc}^{\Lambda}(\boldsymbol{r}) - (E_\Lambda - \varepsilon_c)\right]\varphi_{j\ell s}^{(\Lambda)}(\boldsymbol{r}) = -\sum_{c\neq c'} U_{cc'}^{\Lambda}(\boldsymbol{r})\varphi_{j'\ell's'}^{(\Lambda)}(\boldsymbol{r}), \tag{8}$$

where ε_c and μ_c denote a channel energy and a reduced mass of the ^{5}Li(J_C)-Λ system for the c channel, respectively. The matrix elements $U_{cc'}^{\Lambda}$ can be systematically evaluated using Racah algebra [37–39]:

$$U_{cc'}^{\Lambda}(r) = \left\langle\left[\Phi_{J_C}^{(^5\mathrm{Li})}, \mathcal{Y}_{j\ell s}^{(\Lambda)}\right]_{J_B}\middle|\hat{U}_\Lambda\middle|\left[\Phi_{J'_C}^{(^5\mathrm{Li})}, \mathcal{Y}_{j'\ell's'}^{(\Lambda)}\right]_{J_B}\right\rangle = \sum_{LSK} C_{LSK}^{J_B}(J_C J'_C)\mathcal{F}_{LSK}^{J_C J'_C}(r), \tag{9}$$

where $\mathcal{Y}_{j\ell s}^{(\Lambda)} = [Y_\ell \otimes X_s]_j$ is the spin-orbit function for Λ, $C_{LSK}^{J_B}(J_C J'_C)$ is a purely geometrical strength factor [37], and $\mathcal{F}_{LSK}^{J_C J'_C}(r)$ is the nuclear form factor for the (α-p)-Λ or (^{3}He-d)-Λ system [38,39]. To compute the CC Green's function $G_{cc'}$ in Eq. (2), we numerically solve the associated CC equation for $G_{cc'}$, which is given by

$$G_{cc'}(E_B) = G_c^{(0)}(E_B)\delta_{cc'} + \sum_{c''} G_c^{(0)}(E_B)U_{cc''}^{\Lambda}G_{c''c'}(E_B), \tag{10}$$

where $G_c^{(0)}$ is the free Green's function for the c channel.

D. Fermi-averaged $K^- n \to \pi^- \Lambda$ amplitudes

In the DWIA calculations, considering nuclear medium effects is crucial in nuclear (K^-, π^-) reactions [40,41] because narrow Y^* resonances serve as intermediate states in the $K^- n \to \pi^- \Lambda$ processes. The "in-medium" differential laboratory cross sections for the $K^- n \to \pi^- \Lambda$ reactions in the nucleus are approximately estimated as

$$\left(\frac{d\sigma}{d\Omega}\right)_{\mathrm{lab}} = \beta|\overline{f}_{K^- n\to\pi^-\Lambda}|^2, \tag{11}$$

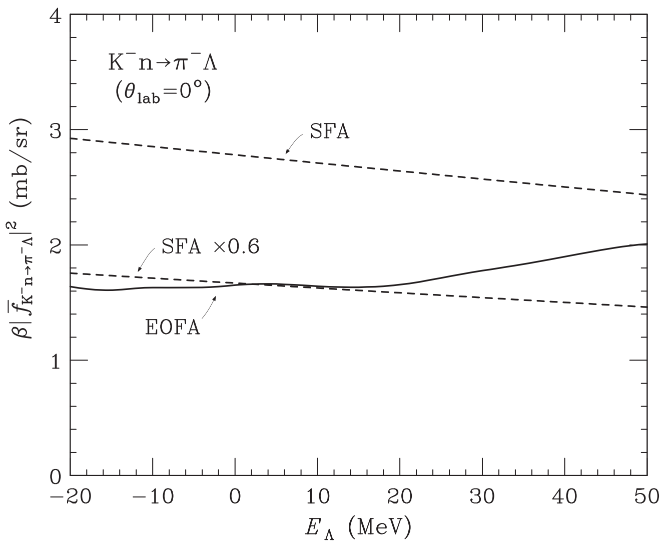

FIG. 3. Fermi-averaged $K^-n \to \pi^-\Lambda$ differential cross sections of $\beta|\overline{f}_{K^-n\to\pi^-\Lambda}|^2$ at $p_{K^-} = 790$ MeV/c and $\theta_{\rm lab} = 0^\circ$, as a function of E_Λ measured relative to the ^{5}Li(g.s.) + Λ threshold. The solid and dashed curves denote the values calculated by EOFA and SFA, respectively, using the elementary $K^-n \to \pi^-\Lambda$ amplitudes given by Gopal *et al.* [42].

where $\overline{f}_{K^-n\to\pi^-\Lambda}$ represents the Fermi-averaged $K^-n \to \pi^-\Lambda$ amplitude. Note that nuclear (K^-, π^-) reactions at $p_{K^-} \simeq 700$–800 MeV/c and $\theta_{\rm lab} \simeq 0^\circ$ occur under near-recoilless conditions, characterized by a small momentum transfer of $q \simeq 60$–80 MeV/c [5,6]. We have difficulties satisfying the on-energy-shell $K^-n \to \pi^-\Lambda$ processes in the optimal Fermi-averaging [26] to evaluate the values of $\overline{f}_{K^-n\to\pi^-\Lambda}$ using the elementary $K^-n \to \pi^-\Lambda$ amplitudes provided by Gopal *et al.* [42]. To overcome the difficulties, therefore, we must require the extended optimal Fermi-averaging (EOFA) method [27] in this calculation.

Figure 3 shows the Fermi-averaged $K^-n \to \pi^-\Lambda$ differential cross sections of $\beta|\overline{f}_{K^-n\to\pi^-\Lambda}|^2$ obtained using EOFA at 790 MeV/c and $\theta_{\rm lab} = 0^\circ$ [27], as a function of E_Λ, along with results from the standard Fermi-averaging (SFA) [41], which incorporates nucleon binding effects. The energy dependence of $\beta|\overline{f}_{K^-n\to\pi^-\Lambda}|^2$ is relatively weak, while the magnitude of EOFA is almost half that of SFA. This result confirms that EOFA is essential for resolving discrepancies between theoretical and experimental angular distributions for ^{12}C$(K^-, \pi^-)^{12}_{\Lambda}$C reactions at $p_{K^-} = 800$ MeV/c [43,44]. Consequently, we expect that the EOFA-derived Fermi-averaged $K^-n \to \pi^-\Lambda$ amplitudes will also be applicable to ^{6}Li(K^-, π^-) reactions.

III. Λ-NUCLEUS POTENTIALS

To examine Λ-nucleus dynamics, the CC Green's function $G_{c'c}$ is obtained by numerically solving the CC equation with a Λ-nucleus (optical) potential $\hat{U}_\Lambda$, which is expressed as

$$\hat{U}_\Lambda(\boldsymbol{r}) = U_0^\Lambda(\boldsymbol{r}) + U_1^\Lambda(\boldsymbol{r})\boldsymbol{I}\cdot\boldsymbol{S}, \qquad (12)$$

where $\boldsymbol{I}$ and $\boldsymbol{S}$ denote the spin operators for the ^{5}Li nuclear core and the Λ, respectively, and $U_s^\Lambda(\boldsymbol{r})$ is obtained using a folding-model potential procedure,

$$U_s^\Lambda(\boldsymbol{r}) = \int \bar{v}_{\Lambda N}^{(s)}(\boldsymbol{r}-\boldsymbol{r}')\rho_s^{(^5{\rm Li})}(\boldsymbol{r}')d\boldsymbol{r}', \qquad (13)$$

where $\bar{v}_{\Lambda N}^{(s)}$ and $\rho_s^{(^5{\rm Li})}$ denote the ΛN effective interaction and the ^{5}Li nuclear density for the nonspin ($s = 0$) or spin ($s = 1$) state, respectively. We omit the spin-orbit $\boldsymbol{L}\cdot\boldsymbol{S}$ term, as it is well known that the Λ spin-orbit potential is small [16,17].

The density $\rho_s^{(^5{\rm Li})}$ is constructed from the α-p or ^{3}He-d cluster wave function [30], reproducing the charge radii of ^{5}Li(g.s.), ^{3}He, and d. When the nuclear shrinkage effect due to the Λ is enhanced in the ^{3}He-d system, the distance D between the ^{3}He and d clusters is expected to decrease upon the addition of a Λ; the value of D should be adjusted to fit the experimental data of $^6_\Lambda$Li(1^+) from the (K^-, π^-) spectrum. Here we take $D = 1.8$ fm using the ^{3}He-d cluster potentials [45], which corresponds to a rms radius of $\langle R^2\rangle^{1/2} = 2.18$ fm between the ^{3}He and d clusters, compared with $\langle R^2\rangle^{1/2} = 2.44$ fm and 2.02 fm for 1_1^+ and 1_2^+ states of $^6_\Lambda$Li, respectively, obtained in the ^{3}He + d + Λ three-body model [21].

The ΛN effective interaction for this model space is represented by a single Gaussian form [19–21]:

$$v_{\Lambda N}(\boldsymbol{r}) = v_{\Lambda N}^0(1+\eta\boldsymbol{\sigma}_N\cdot\boldsymbol{\sigma}_\Lambda)\exp\{-(\boldsymbol{r}/b)^2\}, \qquad (14)$$

with $v_{\Lambda N}^0 = -21.19$ MeV, $b = 1.49$ fm, and $\eta = -0.072$. The range parameter b is determined to reproduce the ΛN scattering data at low energies [46], while the potential strength $v_{\Lambda N}^0$ is adjusted to reproduce the Λ binding energy of 4.50 MeV [10] for $^6_\Lambda$Li(g.s.) within the folding-model potential. The parameter η implies that the spin-singlet ΛN state ($S_<$) is more attractive than the spin-triplet ΛN state ($S_>$) [19–21,47,48]. Using folding-model potentials with a size parameter of $b_N = 1.61$ fm, we calculated the Λ binding energies (B_Λ) to be 1.90 MeV for $^4_\Lambda$He(0^+), 1.25 MeV for $^4_\Lambda$He(1^+), and 0.04 MeV for $^3_\Lambda$H$(1/2^+)$, compared with the corresponding experimental values of 2.39 ± 0.07 MeV, 0.94 ± 0.04 MeV, and 0.13 ± 0.09 MeV [49], respectively. The parameters of the ΛN effective interaction in Eq. (14) are adjusted to reproduce the experimental binding energy of $^6_\Lambda$Li (g.s.), thereby incorporating the main effects of dispersion, Pauli blocking, rearrangement, and Λ-Σ coupling within the two-body YN dynamics. The energy dependence of the Λ-nucleus potential, arising from an effective mass μ^* [50], is neglected here for simplicity. Since the three-body YNN force arising from ΛN-ΣN coupling is not explicitly included, the fine structure of the binding energies of $^4_\Lambda$He(0^+), $^4_\Lambda$He(1^+), and $^3_\Lambda$H$(1/2^+)$ is not fully reproduced. Nevertheless, the present folding-model approach remains sufficient for a phenomenological analysis of Λ production, as shown in Sec. IV.

Figure 4 presents the real parts of the Λ folding-model potentials for $^6_\Lambda$Li with $J_B = 1^-$ and 2^- in the (α-p)-Λ channels, as well as for $J_B = 1^+$, which includes ^{5}Li$(3/2^+) \otimes (0s_{1/2})_\Lambda$ and ^{5}Li$(1/2^+) \otimes (0s_{1/2})_\Lambda$ components in the (^{3}He-d)-Λ channels. The shapes of these potentials are very similar,

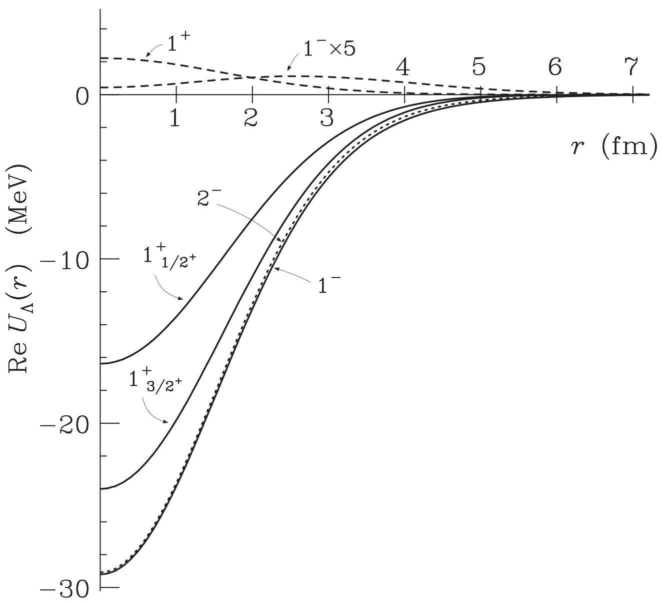

FIG. 4. Real parts of Λ folding-model potentials for several spin J_B states in the ^{5}Li-Λ system, as a function of the relative distance r between the center of mass of ^{5}Li(J_C) and the Λ. Solid curves denote the diagonal potentials for $J_B = 1^-$ in (α-p)-Λ channels and for $J_B = 1^+$ in (^{3}He -d)-Λ channels; a dotted curve for $J_B = 2^-$ in (α-p)-Λ channels. Dashed curves denote the coupling potentials for $J_B = 1^-$ and 1^+.

but their strengths differ moderately due to the $\boldsymbol{I}\cdot\boldsymbol{S}$ term in Eq. (12). For 1^-, the coupling term is small because the valence $0p_{1/2}$ proton in ^{5}Li($1/2^-$) is far from the α core in the (α-p)-Λ system. For 1^+, on the other hand, the Λ diagonal potential for ^{5}Li($3/2^+$) is more attractive than that for ^{5}Li($1/2^+$) because $U_1^\Lambda\langle\boldsymbol{I}\cdot\boldsymbol{S}\rangle$ is attractive (repulsive) for the former (latter), where $U_1^\Lambda > 0$ and $\langle\boldsymbol{I}\cdot\boldsymbol{S}\rangle = J_B(J_B+1) - J_C(J_C+1) - 3/4$. This result mainly stems from the nature of the ΛN effective interaction. Therefore, we confirm that the spin effects arising from the $\boldsymbol{I}\cdot\boldsymbol{S}$ term play a crucial role in the Λ fine structure and spectroscopy of $^6_\Lambda$Li [19,20,47].

IV. RESULTS

A. Energy levels of $^6_\Lambda$Li

We discuss the eigenstates of $^6_\Lambda$Li obtained by solving the CC equations with the Λ-nucleus potentials given in Eq. (12) for ^{5}Li(J_C)-Λ systems within the (α-p)-Λ and (^{3}He -d)-Λ model spaces. Table II presents the calculated energies and widths of the Λ-bound and resonance states with $[^5\text{Li}(J_C)\otimes j_\Lambda]_{J_B}$ in $^6_\Lambda$Li.

For (α-p)-Λ configurations, the 1^- ground state (g.s.) is found at $E_\Lambda = -4.51$ MeV, and the 2^- excited state (exc.) at $E_\Lambda = -4.26$ MeV, both lying below the ^{5}Li(g.s.) + Λ threshold. These 1^-(g.s.) and 2^-(exc.) bound states are unstable due to their strong interaction decay into $^5_\Lambda$He $+p$, located at $E_\Lambda = -5.08$ MeV. The spin-spin coupling between ^{5}Li($3/2^-$) and ^{5}Li($1/2^-$) with Λ for the 1^-(g.s.) is not so significant because the $\boldsymbol{I}\cdot\boldsymbol{S}$ coupling potential is small, as mentioned in Sec. III.

The nature of a bound or resonance state is often determined by the pole position of the S matrix in an n-channel coupled system, where the 2^n Riemann sheets are characterized by n signs of $[\text{Im}k_1\,\text{Im}k_2\cdots\text{Im}k_n]$ with the center-of-mass momentum $k_c = (k_1, k_2, \ldots, k_n)$ in the complex k plane. Thus, the complex energy $\mathcal{E}_\Lambda$ can be expressed as

$$\mathcal{E}_\Lambda = \frac{k_c^2}{2\mu_c} + \Delta_c = E_\Lambda - i\frac{1}{2}\Gamma, \tag{15}$$

where Δ_c denotes the c channel threshold energy measured from the ^{5}Li(g.s.) + Λ threshold. For $J_B = 1^+$, we find the p-wave poles of the S matrix in the $n = 2$ coupled system that mainly consists of $^5\text{Li}(3/2^-)\otimes(0p_{3/2})_\Lambda$ and $^5\text{Li}(3/2^-)\otimes(0p_{1/2})_\Lambda$ configurations on the $[-+]$ and $[--]$ Riemann sheets. In Fig. 5, we illustrate the pole structure for $J_B = 1^+$ near the ^{5}Li(g.s.) + Λ threshold on the $[--]$ sheet in the complex E plane [51,52]. The 1^+_1 pole is located at $\mathcal{E}_\Lambda = -0.45 - i0.98$ MeV on the $[--]$ sheet, which is identified as a $0p_\Lambda$ (decaying) resonance. Because the Λ-nucleus potential has an imaginary part of -0.6 MeV due to the unstable ^{5}Li(g.s.) core, this pole shifts closer to the threshold and behaves like a virtual state. A continuum state for 1^+ shows an enhancement above the threshold (2–3 MeV) by the nearby 1^+_1

TABLE II. Energies and widths of the Λ bound and resonance states of $^6_\Lambda$Li in the ^{5}Li(J_C)-Λ system, together with the experimental data [10]. These values are obtained from pole positions of the S matrix in the complex E plane. The energies in parentheses are measured from the ^{3}He + d + Λ threshold.

State	Configurations		E_Λ^{cal}	Γ^{cal}	Sheet	E_Λ^{exp}	Γ^{exp}
J_B^P	^{5}Li(J_C)	$(n\ell)_{j_\Lambda}$	(MeV)	(MeV)		(MeV)	(MeV)
(α-p)-Λ							
1^-	$3/2^-, 1/2^-$	$0s_{1/2}$	−4.51	1.2	[++]	}−4.50	
2^-	$3/2^-$	$0s_{1/2}$	−4.26	1.2	[+]		
1^+_1	$3/2^-, 1/2^-$	$0p_{3/2}, 0p_{1/2}$	−0.45	0.98	[−−]	} 3.8	
1^+_2	$3/2^-, 1/2^-$	$1p_{3/2}, 1p_{1/2}$	3.1	5.6	[−−]		
(^{3}He -d)-Λ							
1^+_1	$3/2^+, 1/2^+$	$0s_{1/2}$	13.7 (−2.7)	0.2	[++]	} 13.8	0.7 ± 1.0
1^+_2	$3/2^+, 1/2^+$	$0s_{1/2}$	16.3 (−0.18)	0.2	[++]		

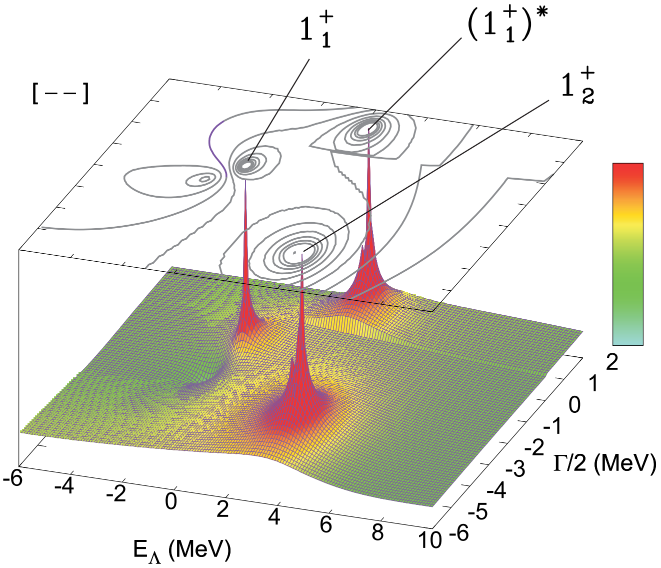

FIG. 5. Pole positions for the $J_B = 1^+$ states in the complex E plane [51,52], using a two-channel coupled system with ^{5}Li$(3/2^-) \otimes (0p_{3/2})_\Lambda$ and ^{5}Li$(3/2^-) \otimes (0p_{1/2})_\Lambda$ channels within the $(\alpha$-$p)$-Λ model space. Poles for 1^+_1 and 1^+_2 reside at $\mathcal{E}_\Lambda = -0.45 - i0.98$ MeV and $\mathcal{E}_\Lambda = 3.1 - i2.8$ MeV on the [−−] Riemann sheet, respectively. A pole for $(1^+_1)^*$ is a partner pole associated with the 1^+_1 pole.

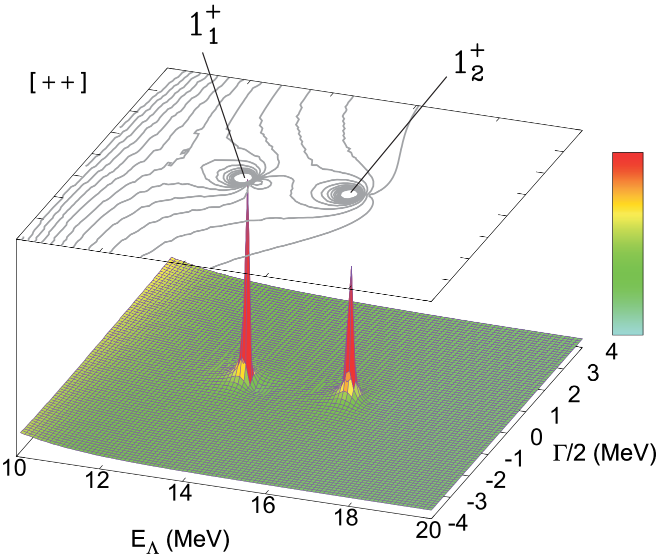

FIG. 6. Pole positions for the $J_B = 1^+$ states in the complex E plane [51,52], using a two-channel coupled system with ^{5}Li$(3/2^+) \otimes (0s_{1/2})_\Lambda$ and ^{5}Li$(1/2^+) \otimes (0s_{1/2})_\Lambda$ channels within the $(^3$He-$d)$-Λ model space. Poles for 1^+_1 and 1^+_2 reside at $\mathcal{E}_\Lambda = 13.7 - i0.1$ MeV and $\mathcal{E}_\Lambda = 16.3 - i0.1$ MeV on the [++] Riemann sheet, respectively.

pole. As a result, the shape of the spectrum changes near the threshold [23]. On the other hand, the $(1^+_1)^*$ pole is a partner of the 1^+_1 pole, which corresponds to a $0p_\Lambda$ (capturing or UBS [23]) resonance, originating from a p-wave conjugate pole associated with the 1^+_1 pole, not observable in the spectrum due to its large distance from the physical axis [23].

Moreover, we find the 1^+_2 pole at $\mathcal{E}_\Lambda = 3.1 - i2.8$ MeV on the [−−] sheet, which is identified as an excited $1p_\Lambda$ resonance pole in the S matrix trajectory obtained using complex potentials, as discussed by Dabrowski [53]. However, this pole shifts far from the physical axis due to the imaginary potential, resulting in a broad width of $\Gamma \simeq 5.6$ MeV in the Λ continuum. These results suggest that the $J_B = 1^+$ state above the ^{5}Li(g.s.) + Λ threshold does not form a broad resonance but rather constitutes a continuum state influenced by nearby poles. This state has perhaps been identified as a substitutional $(0p,\ 0p^{-1})_{\Lambda n}$ state within shell models and cluster models [14,19,20]. Therefore, we conclude that the broad peak at 3.8 MeV shown in Fig. 1 corresponds to a continuum state influenced by nearby poles.

For $(^3$He-$d)$-Λ configurations, two poles, 1^+_1 and 1^+_2, exist at $\mathcal{E}_\Lambda = 13.7 - i0.1$ MeV and $16.3 - i0.1$ MeV, respectively, close to the physical axis, as shown in Table II. Owing to the weak coupling between the $(^3$He-$d)$-Λ and $(\alpha$-$p)$-Λ channels [14], the 1^+_1 and 1^+_2 states may approximately behave as Λ quasibound states, which have ^{5}Li$(3/2^+) \otimes (0s_{1/2})_\Lambda$ and ^{5}Li$(1/2^+) \otimes (0s_{1/2})_\Lambda$ components, on the [++] Riemann sheet below the ^{3}He + d + Λ threshold. The 1^+_1 state is located at $E_\Lambda = 13.7$ MeV, corresponding to $E_\Lambda - E_{\rm th} = -2.7$ MeV near the ^{3}He + d + Λ threshold, where $E_{\rm th} = 16.39$ MeV represents the ^{3}He + d threshold energy measured from the ^{5}Li(g.s.), as shown in Fig. 2. This state is identified as a Λ quasibound state having the rms radius of $\langle r^2_\Lambda \rangle^{1/2} = 3.2$ fm, where the mixing probability of ^{5}Li$(1/2^+)$ into ^{5}Li$(3/2^+)$ for 1^+_1 amounts to 6.8% due to the $\boldsymbol{I} \cdot \boldsymbol{S}$ coupling, which is comparable to 6% obtained in the ^{3}He + d + Λ cluster model [21]. The 1^+_2 state is located at $E_\Lambda = 16.3$ MeV, corresponding to $E_\Lambda - E_{\rm th} = -0.18$ MeV, and is identified as a loosely Λ quasibound state with a large distance of $\langle r^2_\Lambda \rangle^{1/2} = 6.1$ fm. Figure 6 illustrates the pole structures for $J_B = 1^+$ near the ^{3}He + d + Λ threshold on the [++] Riemann sheet [51,52].

B. Comparison with the experimental data

We analyze the Λ production spectrum for the (K^-, π^-) reaction on a ^{6}Li target in the DWIA with the Fermi-averaged $K^- n \to \pi^- \Lambda$ amplitudes obtained by EOFA. Because a nuclear (K^-, π^-) reaction is exothermic, this reaction satisfies under a near-recoilless condition by controlling a momentum transfer [5,6]. For K^- beams at $p_{K^-} = 700$–800 MeV/c and $\theta_{\rm lab} = 0^\circ$, the momentum transfer is $q = 50$–80 MeV/c and $q \simeq 51$ MeV/c at the Λ production threshold, leading to that the angular-momentum transfer $\Delta L = 0$ dominates. For a ^{6}Li$(1^+;$ g.s.) target nucleus, therefore, the substitutional states having $J_B = 1^+$ are expected to be predominantly populated in Λ hypernuclear states [5–9].

Figure 7 displays the calculated inclusive π^- spectrum for Λ production via the ^{6}Li(K^-, π^-) reaction at $p_{K^-} = 790$ MeV/c and $\theta_{\rm lab} = 0^\circ$, together with the experimental data [10]. The calculated spectrum considers a detector resolution of 4 MeV FWHM. The shape of the calculated spectrum agrees well with the data across the entire Λ production

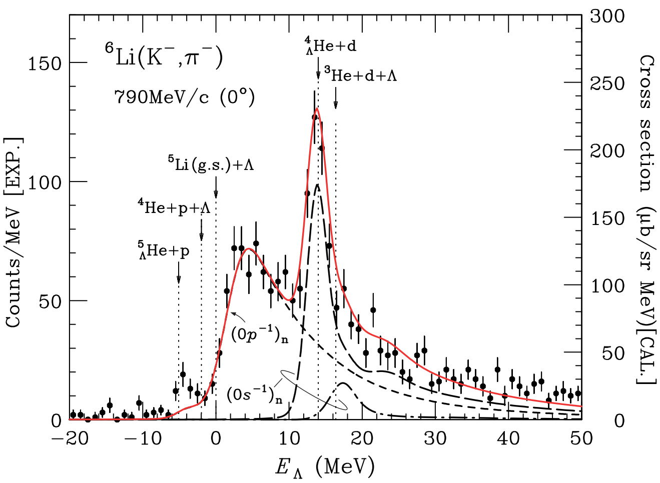

FIG. 7. Calculated inclusive π^- spectrum for Λ production via the ^{6}Li(K^-, π^-) reaction at $p_{K^-} = 790$ MeV/c and $\theta_{\rm lab} = 0^\circ$, together with the experimental data [10], as a function of E_Λ measured relative to the ^{5}Li(g.s.) + Λ threshold. Solid, dashed and long-dashed curves denote neutron-hole contributions of the total, $0p^{-1}$, and $0s^{-1}$, respectively, using $\overline{f}_{K^-n\to\pi^-\Lambda}$ obtained by EOFA [27]. A dot-dashed curve denotes an additional contribution formed by a direct $^4_\Lambda$He $+d$ reaction. These spectra are considered by a detector resolution of 4 MeV FWHM.

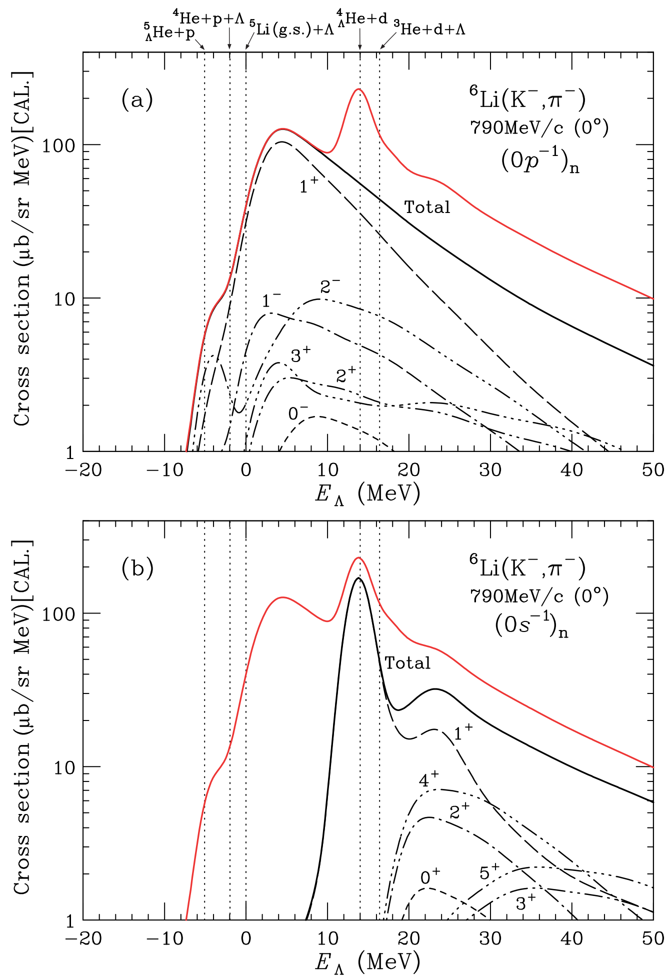

FIG. 8. Partial spin J^P contributions of $^6_\Lambda$Li hypernuclear states from neutron (a) $0p^{-1}$ and (b) $0s^{-1}$ components, to the Λ production spectra in ^{6}Li(K^-, π^-) reactions at 790 MeV/c and $\theta_{\rm lab} = 0^\circ$. These components are obtained in (α-p)-Λ and (^{3}He -d)-Λ configurations, respectively. The spectra are considered with a detector resolution of 4 MeV FWHM.

region, except for a small peak in the Λ bound region. Furthermore, it should be noted that the absolute values of the magnitude of the calculated spectrum are approximately half smaller than that suggested by the experimental data [7–9]. This situation suggests a similar trend to that theoretical values obtained using EOFA for the angular distributions can reproduce the data of the ^{12}C(K^-, π^-)$^{12}_\Lambda$C reaction measured by the BNL experiments [43], as discussed in a previous work [27]. Therefore, we show that the calculated spectra predict the data of the ^{6}Li(K^-, π^-)$^6_\Lambda$Li reaction.

V. DISCUSSION

A. Partial spin components in the spectrum

Figure 8 shows the contributions from neutron $0p^{-1}$ and $0s^{-1}$ states to the inclusive π^- spectrum shown in Fig. 7. We estimate the partial spin J^p contributions of the Λ production for the corresponding (α-p)-Λ and (^{3}He -d)-Λ configurations, as discussed in the following subsections.

1. (α-p)-Λ spectra

For low-lying states with (α-p)-Λ configurations, the cross section of the $J_B = 2^-$(exc.) state at $E_\Lambda = -4.26$ MeV dominates below the ^{5}Li(g.s.) + Λ threshold, as shown in Fig. 8(a). In contrast, the cross section of the 1^-(g.s.) state at $E_\Lambda = -4.51$ MeV is negligible in the Λ bound region due to the suppressed Λ production amplitude, resulting from an admixture of both $(0p_{3/2},\ 0s^{-1}_{1/2})_{\Lambda n}$ and $(0p_{1/2},\ 0s^{-1}_{1/2})_{\Lambda n}$ components. This situation may correspond to an admixture of $S_>$ and $S_<$ states as suggested by cluster-model calculations [19,20]. Since the 2^-(exc.) component dominates in the Λ bound region, the small peak observed at $E_\Lambda \simeq -4.50$ MeV in the data is interpreted as the 2^-(exc.) state. This result is consistent with that obtained in cluster-model calculations [19,20]. However, our calculations do not well reproduce the pronounced small peak, assuming a detector resolution of 4 MeV FWHM.

The cross section for the 1^+(exc.) state associated with ^{5}Li(g.s.) ⊗ $0p_\Lambda$, which corresponds to the $(0p,\ 0p^{-1})_{\Lambda n}$ substitutional component, is predominantly populated. This state manifests as a broad peak at $E_\Lambda \simeq 5.0$ MeV above the ^{5}Li(g.s.) + Λ threshold, as shown in Fig. 7. The poles for 1^+(exc.) are located on the unphysical sheet [−−] at $\mathcal{E}_\Lambda = -0.45 - i0.98$ MeV close to the threshold, and at $\mathcal{E}_\Lambda = 3.1 - i2.8$ MeV which exhibits a broad width and lies far from the physical axis, as discussed in Sec. IV A. This suggests that the broad peak of the 1^+ state stems from Λ continuum states influenced by the nearby poles. This result highlights the crucial role of continuum effects in Λ production, as observed in the π^- spectra [23], indicating that bound-state approximations are insufficient for accurately describing continuum spectra

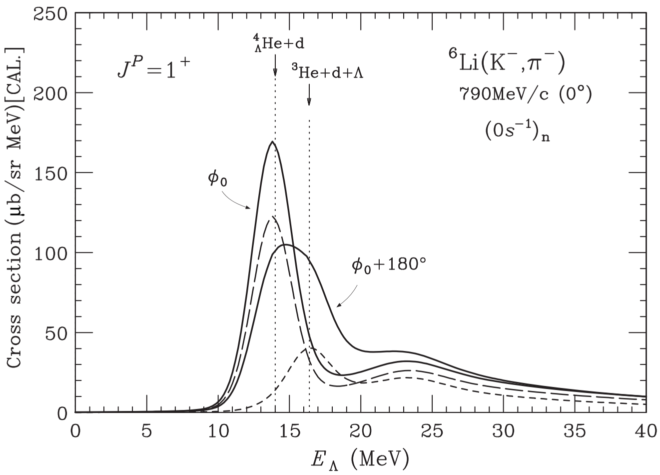

FIG. 9. Interference effects of the Λ production for $J^P = 1^+$ near the $^3\text{He} + d + \Lambda$ threshold on the $^6\text{Li}(K^-, \pi^-)$ reaction at $p_{K^-} = 790$ MeV/c and $\theta_{\text{lab}} = 0^\circ$. The solid curves denote the total spectra changing the relative phases of $\phi = \phi_0$ and $\phi_0 + 180^\circ$ between T_3 and T_1 amplitudes. The long-dashed and dashed curves denote the contributions of $|T_3|^2$ and $|T_1|^2$, respectively. The spectra are considered with a detector resolution of 4 MeV FWHM.

[19–21]. Therefore, a rigorous approach, such as the Green's function method [23], is crucial for a precise analysis of Λ production spectra in nuclear (K^-, π^-) reactions. This approach facilitates a comprehensive description of Λ-nucleus dynamics, including both bound and continuum states.

2. (^{3}He-d)-Λ *spectra*

For high-lying states with (^{3}He-d)-Λ configurations, the cross section for the $J_B = 1^+$ state is predominantly populated, which exhibits a narrow peak ($\Gamma^{\text{exp}} \simeq 0.7 \pm 1.0$ MeV) near the $^4_\Lambda\text{He} + d$ threshold, as shown in Fig. 8(b). Other higher-spin J^P states are rarely populated. This component with $J^P = 1^+$ originates from $^5\text{Li}(3/2^+) \otimes (0s_{1/2})_\Lambda$ and $^5\text{Li}(1/2^+) \otimes (0s_{1/2})_\Lambda$ configurations, corresponding to nearly pure $(0s,\ 0s^{-1})_{\Lambda n}$ substitutional states due to the small momentum transfer $q \simeq 50$–80 MeV/c. To examine the contributions of the 1^+_1 and 1^+_2 states, whose poles reside at $E_\Lambda = 13.7$ and 16.3 MeV in Table II, respectively, we consider the double-differential cross section for 1^+(exc.) in Eq. (1), which can be expressed as

$$\frac{d^2\sigma(1^+)}{d\Omega dE} \propto |T_3|^2 + |T_1|^2 + 2\text{Re}(T_3^* T_1), \qquad (16)$$

where T_3 and T_1 represent the Λ production amplitudes for $^5\text{Li}(3/2^+) \otimes (0s_{1/2})_\Lambda$ and $^5\text{Li}(1/2^+) \otimes (0s_{1/2})_\Lambda$ components, respectively, and the relative phase between them is given by $\phi_0 = \text{Arg}(T_3^* T_1)$. In Fig. 9, we present several spectra of the 1^+ cross section by artificially modifying the relative phases to $\phi = \phi_0$ and $\phi_0 + 180^\circ$ in the interference term $2\text{Re}(T_3^* T_1)$ in Eq. (16), along with the individual contributions of $|T_3|^2$ and $|T_1|^2$. The interference term modifies the spectrum, resulting in a narrower peak shape near the $^3\text{He} + d + \Lambda$ threshold, although both 1^+_1 and 1^+_2 states contribute to the Λ production. Additionally, we observe a broad shoulder in 1^+ around $E_\Lambda = 24$ MeV, as shown in Fig. 8(b), which originates from the $^5\text{Li}(3/2^+, 1/2^+) \otimes (0d_{5/2,3/2})_\Lambda$ configurations obtained from the (^{3}He-d)-Λ cluster potentials.

3. $^4_\Lambda$He + d *spectra*

It is worthwhile to note that light nuclear targets such as ^{6}Li have played an essential role as a doorway for producing various hyperfragments, including $^5_\Lambda$He, $^4_\Lambda$He, $^4_\Lambda$H, and $^3_\Lambda$H, via the (K^-, π^-) reactions [14]. To examine the contribution of a $^4_\Lambda\text{He} + d$ process, which corresponds to the direct production of a $^4_\Lambda$He hyperfragment [54], we estimate the cross section for $^4_\Lambda\text{He} + d$ production via the reaction $K^- + {}^6\text{Li} \to \pi^- + {}^4_\Lambda\text{He} + d$ at $p_{K^-} = 790$ MeV/c and $\theta_{\text{lab}} = 0^\circ$, using the form factor $F_\alpha(q)$ for a ^{4}He target within a DWIA calculation [55,56]. In Fig. 7, we have presented the π^- spectra at $p_{K^-} = 790$ MeV/c and $\theta_{\text{lab}} = 0^\circ$, including contributions from the $^4_\Lambda\text{He} + d$ component, along with those from the (α-p)-Λ and (^{3}He-d)-Λ components. The contribution of the $^4_\Lambda\text{He} + d$ component in the (K^-, π^-) reaction at $p_{K^-} = 790$ MeV/c and $\theta_{\text{lab}} = 0^\circ$ is not so significant, as the continuum states associated with $^4_\Lambda\text{He} + d$ are naturally suppressed due to the small momentum transfer of $q \simeq 50$–80 MeV/c in this substitutional reaction.

B. Effects of the three-body *YNN* force and Σ admixture

The high-lying excited states of $^6_\Lambda$Li appear to be promising candidates for investigating the three-body YNN force involving ΛNN-ΣNN coupling induced by the ΛN-ΣN interaction, rather than the Fujita-Miyazawa-type ΛNN force, which is expected to have only a minor impact on the energies in free space. In the (^{3}He-d)-Λ configuration, the $^3\text{He} + \Lambda$ subsystem is coupled with $^3\text{H} + \Sigma^+$ and $^3\text{He} + \Sigma^0$ in $^4_\Lambda$He via the ΛNN-ΣNN interaction caused by coherent Λ-Σ coupling [25,57], and the $d + \Lambda$ subsystem is coupled with $\{nn\}\Sigma^+$, $\{pn\}\Sigma^0$, and $\{pp\}\Sigma^-$ in $^3_\Lambda$H [58]. Therefore, the three-body YNN force is expected to play a crucial role in determining the fine structure of the excited (^{3}He-d)-Λ states, depending on the spin-isospin states in $^5\text{Li}(J_C)$-Λ/Σ. However, the present analysis cannot resolve the energy shifts of the fine Λ states, as the experimental spectra were measured with a resolution of approximately 4 MeV FWHM [10]. To clarify the effects of the YNN force in this nucleus, high-resolution measurements at dedicated beamlines are required.

Moreover, Λ-Σ coupling induces a Σ admixture in the wave functions of Λ hypernuclear states [59]. These Σ components can also be populated through direct processes such as $K^- p \to \pi^- \Sigma^+$ and $K^- n \to \pi^- \Sigma^0$, which provide direct access to the Σ admixture in the nucleus [60]. However, this effect is expected to be negligible in the nuclear (K^-, π^-) reaction at $p_{K^-} = 790$ MeV/c, as the Fermi-averaged amplitudes $\overline{f}_{K^-p\to\pi^-\Sigma^+}$ and $\overline{f}_{K^-n\to\pi^-\Sigma^0}$ are much smaller than $\overline{f}_{K^-n\to\pi^-\Lambda}$.

C. Comparison with other calculations

Majling *et al.* [14] discussed that the peak at 13.8 MeV in the ^{6}Li(K^-, π^-) data indicates Λ production via $(0s, 0s^{-1})_{\Lambda n}$ with a narrow width of $\Gamma \simeq 0.7 \pm 1.0$ MeV, due to the small admixture between wave functions with $[f] = [411]$ and [321] in spatial symmetry. According to Ref. [14], we approximately neglect the couplings between the (α-p)-Λ and (^{3}He-d)-Λ channels in the CC equation. This assumption is further supported by the small imaginary part of the optical potential for $t + d$ scattering [13,34] and the reduction of events near the peak at 13.8 MeV in the spectrum for proton coincidence via nonmesonic weak decay of $^5_\Lambda$He [12]. Therefore, we conclude that this approximation is valid in our calculations.

Auerbach and Van Giai [22] attempted to calculate continuum spectra within a single-particle Λ description using a ΛN^{-1} basis for ^{6}Li, ^{7}Li, and ^{9}Be targets, revealing the fundamental features of continuum effects in nuclear (K^-, π^-) reactions. They indicated that the peak at 3.5 MeV in $^6_\Lambda$Li does not correspond to a resonance state but rather to a continuum state above the ^{5}Li(g.s.) + Λ threshold. However, their calculated spectra fail to accurately reproduce the experimental data across the entire energy range due to the omission of spin structure in the $^5\mathrm{Li}(J_C) \otimes \Lambda$ configuration. When evaluating the continuum states in the spectra, it is essential to incorporate the spin structure of $^6_\Lambda$Li, as discussed in Sec. IV.

Motoba *et al.* [19,20] investigated the structures and production cross sections in the (K^-, π^-) reaction on a ^{6}Li target using a microscopic $\alpha + p + \Lambda$ cluster model. They analyzed the spin structure in $^6_\Lambda$Li, demonstrating that the $\boldsymbol{\sigma}_N \cdot \boldsymbol{\sigma}_\Lambda$ term plays a crucial role in determining the cross sections. Their findings indicate that the production cross section for the 2^-(exc.) state is larger than that for the 1^-(g.s.) state because the spin $S_>$ and $S_<$ components are significantly mixed only in the 1^-(g.s.) state. The peak at 3.8 MeV has been identified as a broad 1^+ resonance, which does not have a simple shell-model substitutional structure such as $(p_{3/2},\ p^{-1}_{3/2})_{\Lambda n}$. Instead, it exhibits a strong admixture of $^5\mathrm{Li}(3/2^-) \otimes (0p_{3/2})_\Lambda$ and $^5\mathrm{Li}(3/2^-) \otimes (0p_{1/2})_\Lambda$ within the cluster-model framework. However, our results suggest that no broad resonance peak exists for the 1^+(exc.) state, despite the significant role of the spin structure in describing the spectrum data.

Ohkura *et al.* [21] extensively studied the structure and production mechanisms of a high-lying excited state of $^6_\Lambda$Li using a microscopic $^3\mathrm{He} + d + \Lambda$ cluster model. Their calculated energies and widths of the 1^+_1 and 1^+_2 excited states successfully explain the prominent peak at 13.8 MeV observed in the ^{6}Li(K^-, π^-) reaction data. Our results appear to be similar to theirs. However, since their calculations are based on a bound-state approximation, they fail to describe the continuum Λ states accurately above the $^3\mathrm{He} + d + \Lambda$ threshold.

Therefore, to extract valuable insights into the structure and production mechanisms of Λ hypernuclei, it is crucial to compute the Λ production spectra while explicitly incorporating the spin structure of Λ bound, resonance, and continuum states in $^6_\Lambda$Li, as discussed in Sec. IV.

D. Future outlook

It is important to discuss potential improvements in the theoretical framework of our calculations to achieve our goals. One key aspect of such improvements is the consideration of self-consistency in describing the structure of light Λ hypernuclei, particularly for high-lying excited states near the nuclear core breakup thresholds, at which the α cluster breaks into $3N + N$. This consideration is crucial because the shrinkage effects induced by the Λ hyperon [47] can enhance the nuclear core density, requiring more accurate microscopic descriptions of the core states.

The fine structure of high-lying excited states in $^6_\Lambda$Li is important for examining the effects of the three-body YNN force, which involves ΛNN-ΣNN coupling induced by the ΛN-ΣN interaction in the Λ production mechanism. To achieve a comprehensive understanding of such systems, it is also essential to adopt a unified treatment for describing the production reactions of Λ hypernuclei. The reaction channel (^{3}He-d)-Λ involves rearrangement channels corresponding to (^{3}He-Λ)-d. Thus, a consistent theoretical approach to these rearrangement-channel reactions is essential. Moreover, a unified approach to the Λ production reaction in both the (α-p)-Λ and (^{3}He-d)-Λ channels is required to perform a fully coupled calculation that accurately describes the reaction dynamics.

VI. SUMMARY AND CONCLUSION

We have conducted a theoretical investigation of the Λ production spectra via the (K^-, π^-) reaction on a ^{6}Li target, using DWIA with a Fermi-averaged $K^- n \to \pi^- \Lambda$ amplitude obtained through EOFA. We have calculated the Λ bound, resonance, and continuum states in the Green's function method for the ^{5}Li-Λ system by solving the CC equations with the Λ folding-model potentials based on α-p and ^{3}He-d cluster wave functions. We have analyzed the shape and magnitude of the spectra by comparing them with experimental data from the ^{6}Li(K^-, π^-) reaction. Results are summarized as follows:

(1) The calculated spectrum for the (K^-, π^-) reaction at $p_{K^-} = 790$ MeV/c (0°) agrees well with the experimental data, incorporating substitutional $(0p,\ 0p^{-1})_{\Lambda n}$ and $(0s,\ 0s^{-1})_{\Lambda n}$ configurations. It is crucial to consider the spin structure of $^6_\Lambda$Li to accurately evaluate the spectra in the Λ continuum regions.

(2) The two-pole structure for the 1^+_1 and 1^+_2 resonance states emerges near the $^3\mathrm{He} + d + \Lambda$ threshold, where interference effects between $^5\mathrm{Li}(3/2^+) \otimes (0s_{1/2})_\Lambda$ and $^5\mathrm{Li}(1/2^+) \otimes (0s_{1/2})_\Lambda$ modify the Λ production spectrum, leading to a narrower peak at 13.8 MeV for $J^P = 1^+$.

(3) The magnitude of the differential cross sections with the Fermi-averaged $K^- n \to \pi^- \Lambda$ amplitude obtained through EOFA is approximately half that obtained using the SFA. Nevertheless, the absolute values of these cross sections agrees well with the experimental data, effectively resolving the discrepancy between the theories and BNL experimental results.

In conclusion, we have successfully explained the inclusive π^- spectra for Λ production in ${}^{6}_{\Lambda}$Li via the ^{6}Li(K^-, π^-) reaction within the DWIA framework using EOFA, along with the Green's function method and Λ folding-model potentials. Continuum effects, including nuclear spin structure considerations, enable accurate reproduction of the spectral data. This study provides a valuable framework for extracting essential information on the structure and production mechanisms of Λ hypernuclei from experimental data. Further microscopic calculations of Λ-nucleus potentials, based on modern ΛN interactions, are essential for gaining deeper insights into YN and YNN interactions that involve YN short-range correlations [61]. These aspects will be explored in future studies.

ACKNOWLEDGMENTS

The authors thank Dr. A. Dote, Professor Y. Akaishi, and Professor S. Shinmura for their valuable comments. This work was supported by Grants-in-Aid for Scientific Research (KAKENHI) from the Japan Society for the Promotion of Science: Scientific Research (C) (Grant No. JP20K03954).

DATA AVAILABILITY

The data supporting this study's findings are available within the article.

[1] H. Sugimura *et al.* (J-PARC E10 Collaboration), Phys. Lett. B **729**, 39 (2014); R. Honda *et al.* (J-PARC E10 Collaboration), Phys. Rev. C **96**, 014005 (2017).
[2] T. Harada and Y. Hirabayashi, Phys. Rev. C **95**, 044610 (2017).
[3] T. Harada, R. Honda, and Y. Hirabayashi, Phys. Rev. C **97**, 024601 (2018).
[4] H. Fujioka *et al.*, Few-Body Syst. **62**, 47 (2021).
[5] M. I. Podgoretskii, Zh. Éksp. Teor. Fiz. **44**, 695 (1963) [Sov. Phys. JETP **17**, 470 (1963)]; H. Feshbach and A. Kerman, in *Preludes in Theoretical Physics,* edited by A. De-Shalit, H. Feshbach, and L. Van Hove (North-Holland, Amsterdam, 1966), p. 260.
[6] A. K. Kerman and H. J. Lipkin, Ann. Phys. (NY) **66**, 738 (1971).
[7] B. Povh, Rep. Prog. Phys. **39**, 823 (1976).
[8] W. Brückner *et al.*, Phys. Lett. B **62**, 481 (1976).
[9] W. Brückner *et al.* (Heidelberg-Saclay-Strasbourg Collaboration), Phys. Lett. B **79**, 157 (1978).
[10] R. Bertini *et al.* (Heidelberg-Saclay-Strasbourg Collaboration), Nucl. Phys. A **368**, 365 (1981).
[11] R. Bertini *et al.* (Heidelberg-Saclay-Strasbourg Collaboration), Nucl. Phys. A **360**, 315 (1981).
[12] J. J. Szymanski, AIP Conf. Proc. **150**, 934 (1986); J. J. Szymanski *et al.*, Phys. Rev. C **43**, 849 (1991).
[13] V. G. Neudatchin and Yu. F. Smirnov, *Nucleon Clusters in Light Nuclei* (Nauka, Moscow, 1969); V. G. Neudatchin, V. I. Kukulin, V. N. Pomerantsev, and A. A. Sakharuk, Phys. Lett. B **255**, 482 (1991).
[14] L. Majling, M. Sotona, J. Žofka, V. N. Fetisov, and R. A. Eramzhyan, Phys. Lett. B **92**, 256 (1980).
[15] E. H. Auerbach, A. J. Baltz, C. B. Dover, A. Gal, S. H. Kahana, L. Ludeking, and D. J. Millener, Ann. Phys. (NY) **148**, 381 (1983).
[16] H. Bandō, T. Motoba, and J. Žofka, Int. J. Mod. Phys. A **05**, 4021 (1990).
[17] A. Gal, E. V. Hungerford, and D. J. Millener, Rev. Mod. Phys. **88**, 035004 (2016).
[18] D. J. Millener, Lect. Notes Phys. **724**, 31 (2007).
[19] T. Motoba, H. Bandō, and K. Ikeda, Prog. Theor. Phys. **70**, 189 (1983); **71**, 222 (1984).
[20] T. Motoba, H. Bandō, K. Ikeda, and T. Yamada, Prog. Theor. Phys. Suppl. **81**, 42 (1985).
[21] H. Ohkura, T. Motoba, and K. Ikeda, Prog. Theor. Phys. **89**, 437 (1993).
[22] N. Auerbach and N. Van Giai, Phys. Lett. B **90**, 354 (1980).
[23] O. Morimatsu and K. Yazaki, Prog. Part. Nucl. Phys. **33**, 679 (1994).
[24] J. Hüfner, S. Y. Lee, and H. A. Weidenmüller, Nucl. Phys. A **234**, 429 (1974).
[25] T. Harada, Phys. Rev. Lett. **81**, 5287 (1998); Nucl. Phys. A **672**, 181 (2000).
[26] T. Harada and Y. Hirabayashi, Nucl. Phys. A **744**, 323 (2004).
[27] T. Harada and Y. Hirabayashi, Phys. Rev. C **105**, 064606 (2022).
[28] C. B. Dover and A. Gal, Ann. Phys. (NY) **146**, 309 (1983).
[29] T. Koike and T. Harada, Nucl. Phys. A **804**, 231 (2008).
[30] S. Saito, Prog. Theor. Phys. **41**, 705 (1969); H. Furutani *et al.*, Prog. Theor. Phys. Suppl. **68**, 193 (1980).
[31] H. Kanada, T. Kaneko, and Y. C. Tang, Nucl. Phys. A **389**, 285 (1982).
[32] Y. Sakuragi, M. Yahiro, and M. Kamimura, Prog. Theor. Phys. Suppl. **89**, 136 (1986); Prog. Theor. Phys. **70**, 1047 (1983).
[33] H. De Vries, C. W. de Jager, and C. de Vries, At. Data Nucl. Data Tables **36**, 495 (1987).
[34] D. R. Tilley *et al.*, Nucl. Phys. A **708**, 3 (2002).
[35] H. Tyrén *et al.*, Nucl. Phys. **79**, 321 (1966); G. Jacob and Th. A. Maris, Rev. Mod. Phys. **38**, 121 (1966); **45**, 6 (1973); F. P. Brady, N. S. P. King, B. E. Bonner, M. W. McNaughton, J. C. Wang, and W. W. True, Phys. Rev. C **16**, 31 (1977).
[36] F. Ajzenberg-Selove, Nucl. Phys. A **490**, 1 (1988).
[37] N. K. Glendenning, *Direct Nuclear Reactions* (Academic Press, New York, 1983), p. 144.
[38] K. T. R. Davies and G. R. Satchler, Nucl. Phys. A **53**, 1 (1964).
[39] T. Tamura, Rev. Mod. Phys. **37**, 679 (1965).
[40] J. Žofka, M. Sotona, and V. N. Fetisov, Nucl. Phys. A **431**, 603 (1984).
[41] A. S. Rosenthal and F. Tabakin, Phys. Rev. C **22**, 711 (1980).
[42] G. P. Gopal *et al.*, Nucl. Phys. B **119**, 362 (1977).
[43] R. E. Chrien *et al.*, Phys. Lett. B **89**, 31 (1979).
[44] C. B. Dover, A. Gal, G. E. Walker, and R. H. Dalitz, Phys. Lett. B **89**, 26 (1979).
[45] V. Della Rocca, R. Bijker, and F. Iachello, Nucl. Phys. A **966**, 158 (2017); V. Della Rocca and F. Iachello, **973**, 1 (2018).
[46] R. H. Dalitz, R. C. Herndon, and Y. C. Tang, Nucl. Phys. B **47**, 109 (1972); R. H. Dalitz and G. Rajasekaran, Nucl. Phys. **50**, 450 (1964).

[47] E. Hiyama, M. Kamimura, T. Motoba, T. Yamada, and Y. Yamamoto, Phys. Rev. C **53**, 2075 (1996).
[48] Y. Yamamoto, T. Motoba, and T. A. Rijken, Prog. Theor. Phys. Suppl. **185**, 72 (2010), and references therein.
[49] M. Jurič *et al.*, Nucl. Phys. B **52**, 1 (1973).
[50] T. Harada and Y. Hirabayashi, Phys. Rev. C **107**, 054611 (2023).
[51] B. C. Pearce and B. F. Gibson, Phys. Rev. C **40**, 902 (1989).
[52] T. Harada and Y. Hirabayashi, JPS Conf. Proc. **17**, 012008 (2017).
[53] J. Dabrowski, J. Phys G: Nucl. Part. Phys. **23**, 1539 (1997).
[54] H. Tamura *et al.*, Phys. Rev. C **40**, R479 (1989).
[55] T. Harada and Y. Hirabayashi, Phys. Rev. C **100**, 024605 (2019).
[56] T. Harada and Y. Hirabayashi, Nucl. Phys. A **1015**, 122301 (2021).
[57] Y. Akaishi, T. Harada, S. Shinmura, and Khin Swe Myint, Phys. Rev. Lett. **84**, 3539 (2000).
[58] T. Harada and Y. Hirabayashi, Phys. Rev. C **89**, 054603 (2014).
[59] A. Umeya and T. Harada, Phys. Rev. C **79**, 024315 (2009).
[60] T. Harada, A. Umeya, and Y. Hirabayashi, Phys. Rev. C **79**, 014603 (2009).
[61] Y. Kurihara, Y. Akaishi, and H. Tanaka, Prog. Theor. Phys. **67**, 1483 (1982).